The torsion pendulum as a tool to study non-linear oscillations and the transition to deterministic chaos

Andrea Sconza and Giacomo Torzo
Phys Dept. "*G. Galilei*", Padova University, Italy

Introduction

In the traditional physics courses we are used to teach only harmonic oscillations, e.g. those produced by restoring forces that are proportional to the displacement x from equilibrium conditions and by dissipative forces proportional to the velocity dx/dt. Such ideal systems give *free* oscillations whose period does not depend on amplitude (*isochronous* oscillators) and *forced* oscillations whose resonance curve is almost symmetric with respect to the self-frequency.
In the real world, many systems include non-linearity in restoring or dissipative forces, and *non-linearity* leads to completely different behaviours.
The free oscillation frequency becomes strongly dependent on the amplitude, and in forced oscillations the concept itself of resonant frequency becomes fuzzy, because for any given frequency one may observe different kinds of oscillations with different amplitudes; moreover *hysteresis* appears with the phenomenon of *amplitude jumps.*
Finally, the investigation of non-linear forced oscillations helps to understand how a classic (*deterministic*) system may exhibit a *chaotic* behaviour, i.e. unpredictable time evolutions, due to a strong dependence on extremely small changes of initial conditions (*deterministic chaos*).
The simplest way to present to the students the forced non-linear oscillations is the method proposed by the mathematician C. Duffing [1], because it offers approximate analytical solutions.
Duffing studied a system with a (small) cubic term in the restoring force *Fr(x)*
Neglecting dissipative forces we get the equation:

$$M\frac{d^2x}{dt^2} = Fr\,(x) + F\cos(\omega t) = -K'x - K''x^3 + F\cos(\omega t) \qquad (1),$$

where $Fr\,(x) = -K'x - K''x^3$ is the non-linear restoring force, $F\cos(\omega t)$ is the driving force and M the mass. Letting $\alpha = \omega_o^2 = K'/M$ e $\beta = K''/M$ we obtain the simpler form:

$$\frac{d^2x}{dt^2} + \alpha x + \beta x^3 = F/M\cos(\omega t) \qquad (2)$$

Assuming that this equation has stationary sinusoidal solutions, we may, with some approximations [2], obtain a relation between the frequency $\nu = \omega/2\pi$ and the amplitude A:

$$\omega^2 = \alpha + \frac{3}{4}\beta A^2 \pm F/(MA) \qquad (3)$$

The double relation (3) (one corresponding to the sign + and one to the sign -) tells that, for each amplitude A, *two stationary oscillations* are possible, corresponding to different frequencies.
A plot of these two frequencies as functions of amplitude is shown in figure 1.
The double sign in (3) corresponds to different stationary oscillations either *in phase* or *in opposition* with respect to the driving force.

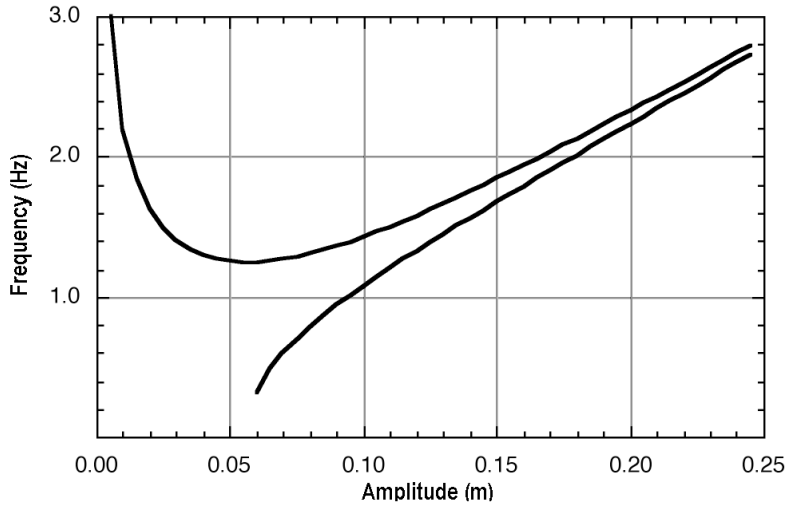

Figure 1: Undamped forced oscillations: frequencies vs. amplitude (here $\alpha = 0.4\ s^{-2}$, $\beta = 160\ m^{-2}s^{-2}$, $F/M = 0.044$ N/kg)

The two curves in Figure 1 never meet, due to the absence of dissipative term in eq. 1. Introducing a dissipative force proportional to velocity, we obtain the equation:

$$\frac{d^2x}{dt^2} + \varepsilon\frac{dx}{dt} + \alpha x + \beta x^3 = F/M\cos(\omega t) \qquad (4),$$

from which a new approximate relation may be derived in place of previous eq. (3):

$$(\omega^2 - \alpha - (3/4)\beta A^2)^2 + \omega^2\varepsilon^2 = F^2/(MA)^2 \qquad (5).$$

This is a biquadratic equation in ω, that (neglecting negative roots, physically meaningless) gives the plot shown in Figure 2, where the two curves meet at a maximum amplitude beyond which no stable oscillation is possible.

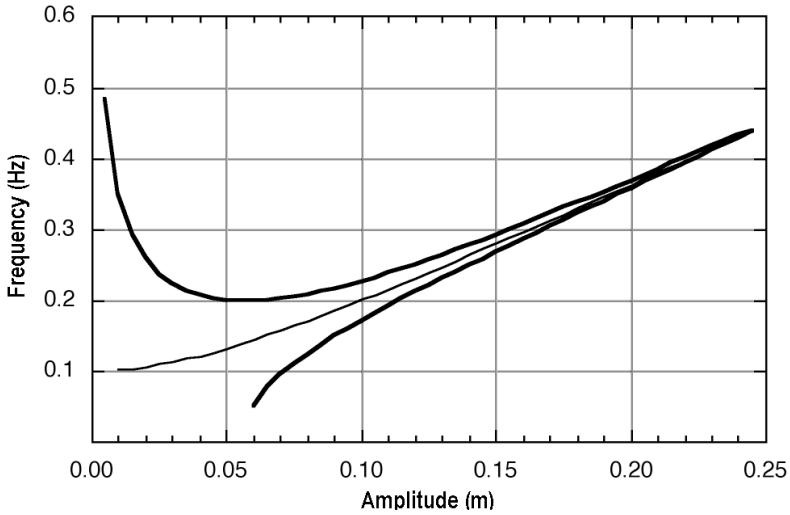

Figure 2: Damped forced oscillations ($\varepsilon = 0.065\ s^{-1}$)

The intermediate curve in figure 2 represents the relation between frequency and amplitude for *free* oscillations, that is obtained from (5) letting F=0 . The departure of this curve from the horizontal straight line measures *anisochronism* of the system.
We note that relations (3) and (5), are *third* order equations in the variable A, and therefore for each frequency there are up to 3 values of the oscillation amplitude

By interchanging the coordinate axes we obtain plots that are commonly named "resonance curves" . The resonance curve predicted by eq. (5) is shown in figure 3: we see that for frequencies between 0.20 Hz and 0.45 Hz there are 3 possible values for the amplitude of forced oscillations.

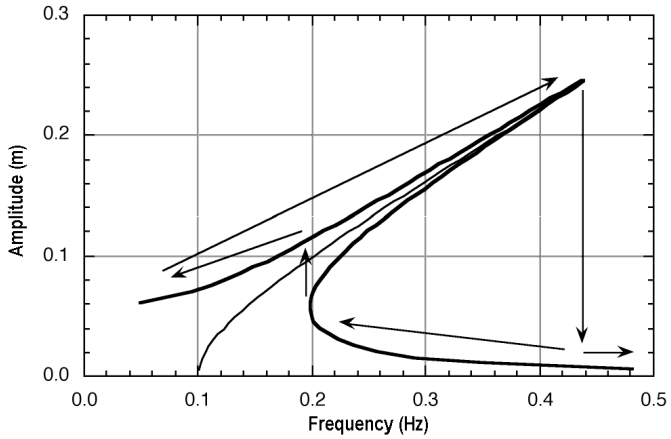

Figure 3: Resonance curve of cubic oscillator with $\beta > 0$ (amplitude jumps are marked by arrows)

The resonance curve, that for linear restoring force is a peak approximately *symmetric* and centred on the self frequency $\omega = \omega_o$, for a cubic restoring force with $\beta > 0$ results *bended to the right side*.

The 3 possible values of the oscillation amplitude produce an hysteretic behaviour. By driving the system with a constant force F , and increasing the frequency ν from small values (in our example about 0.05 Hz) the stationary oscillation amplitude gradually increases following the upper curve of Figure 3 until, at the maximum value, it drops to the lower curve and it stays low if we still increase the frequency.

On the other hand, if we start from high frequency and we decrease it, the amplitude follows the lower curve until we reach the turning point (near 0.20 Hz in our example), where the amplitude makes an upward jump to the upper curve, that is then followed for further reduced frequency.

The upper part of the lower curve in figure 3 cannot be observed experimentally.

This hysteresis phenomenon is known as *amplitude jumps in forced non-linear oscillations*.

By studying an oscillator where $\beta < 0$ we find that the resonance curve is *bended leftward* (figure 4).

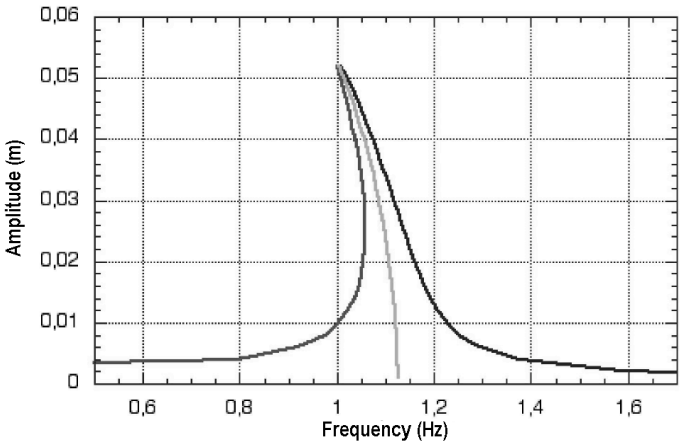

Figure 4: Resonance curve of cubic oscillator with $\beta < 0$ (con $\alpha = 50\ s^{-2}$, $\beta = -5000\ m^{-2}s^{-2}$, $\varepsilon = 0.3\ s^{-1}$, F/M = 0.1 N/kg)

An interesting behaviour is offered by a system where, in the restoring force, the sign of the linear term is positive and that of the cubic term is negative, i.e. ($Fr(x)=+K'x - K'''x^3$, (this leads to $\alpha < 0$ and $\beta > 0$ in the Duffing equation (4)).
In this case there are two stable equilibrium positions, as we may see from the potential energy V(x):

$$V(x)= - \int Fdx = -1/2\ K' x^2 + 1/4\ K''' x^4$$

The plot of V(x) exhibits two minima for $+x_o$ and $-x_o = \pm$ sqrt (K'/K''') instead of a single minimum at $x_o = 0$ as it happens for α and β both positive.
In presence of two minima for the potential energy, we may observe two kinds of oscillations: the normal periodic oscillations around one of the two equilibrium positions, or non-periodic motions in which the body keeps jumping from one region to the other showing a behaviour that seems chaotic.
Actually the behaviour is always deterministic, i.e. , for a given a starting condition, the time evolution is exactly determined by the differential equation (4), but extremely small changes in the initial conditions produce strong changes in the time evolution.
An example of this behaviour is offered by the *inverted* torsion pendulum, made of a mass M attached to the top of a vertical elastic bar with the other end fixed. If the bar elastic constant is less than a critical value, the system has two equilibrium positions: one with the bar flexed leftward and one with the bar flexed rightward.
Here we describe a device that is well suited for investigating both the normal stationary oscillations and the transition to deterministic chaos (by properly adjusting the amplitude and frequency of the driving force). It is a torsion pendulum with two restoring torques: the elastic one, proportional to the displacement θ from equilibrium position, and the gravitational one, due to the weight of an eccentric mass (proportional to $\cos\theta$), that is responsible on non-linearity and, in some situation, may lead to chaos.

1. The experimental apparatus

Our torsion pendulum is a device designed within an Erasmus stage at Padua University of a student from Ljubljana University, Samo Lasic, who wrote his Thesis on this subject [3] and presented it during the 2001 GIREP International Meeting in Udine [4]. A second Thesis, from which most part of the experimental data here reported are taken, was written in Padua by Paola Bedendo [5].

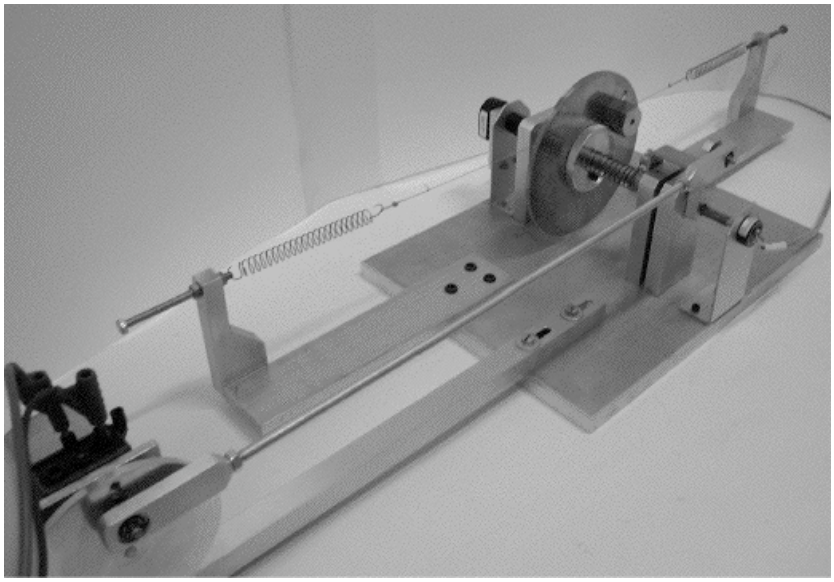

Figure 5: The torsion pendulum

The device is made of a brass disc rotating on horizontal axis (radius r = 7 mm) on ball bearings to reduce friction. A mass M is fixed on the disc at a distance R from axis, that may be adjusted from R_{min}= 43 mm and R_{max}= 64 mm along a radial slot. Two lateral spring are attached to the axis by means of thin wires wound around it, producing torques of opposite signs. (Figure 5). By separately adjusting the spring tensions we may trim the equilibrium position of the mass M.
The disc rotation angle is measured by an optical encoder [6] attached to the axis.
The time evolution of the oscillations is recorded by measuring the rotation angle as a function of time with a constant sampling rate through an interface connected to a Personal Computed via serial cable [7].
The disc, with the eccentric mass, may be turned with respect to its axis and then blocked, thus allowing to achieve the stable equilibrium position ($\theta = 0$) either with the mass M vertically below the axis centre (normal pendulum, figure 6a) or above (inverted pendulum, figure 6b).
In the *normal* pendulum case, the motion equation is:

$$I \frac{d^2\theta}{dt^2} = -MgR\sin\theta - K_{eff}\theta - 2\gamma \frac{d\theta}{dt} \quad , \qquad (6)$$

where I is the inertia momentum, K_{eff} the effective elastic constant and the dissipative term $-2\gamma \frac{d\theta}{dt}$ assumes a friction proportional to the angular velocity .

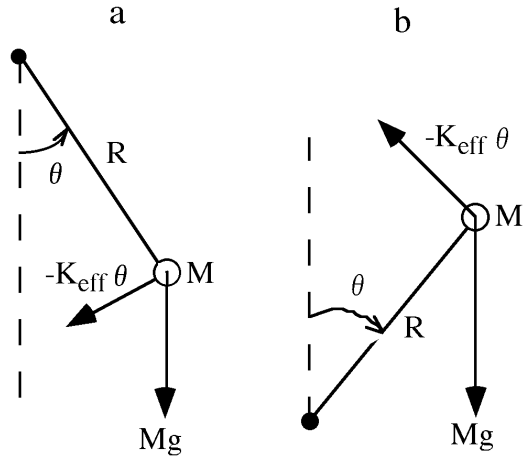

Figure 6: the restoring forces for normal pendulum(a) and inverted pendulum (b)

In the *inverted* pendulum case, the elastic restoring torque, $-K_{eff}\theta$, forces the disc towards the position $\theta = 0$, while the torque due to gravity, $+MgR\sin\theta$, forces the disc in the opposite direction
The motion equation is now:

$$I \frac{d^2\theta}{dt^2} = +MgR\sin\theta - K_{eff}\theta - 2\gamma \frac{d\theta}{dt} \qquad (7),$$

Here we may have two cases. If $MgR < K_{eff}$ (i.e. $\beta>0$) one single equilibrium position exists, with M exactly above the rotation axis ($\theta=0$). If $MgR > K_{eff}$ (i.e. $\beta<0$) two equilibrium positions exist : one at right and one at left , that may be approximately calculated by equating the opposing torques, and using the MacLaurin series expansion ($\sin\theta \approx \theta - 1/6\ \theta^3$):

$$\theta_{1,2} \approx \pm \sqrt{6(1 - K_{eff} / MgR)}, \qquad (8)$$

Alternatively we may use a graphical approach, searching the intersection of the $\sin\theta$ curve with the straight line $y = \left(K_{eff} / MgR\right)\theta$.

In our apparatus M is chosen in order to let $\beta>0$ for $R = R_{min}$ (equilibrium at $\theta=0$) and $\beta<0$ for $R = R_{max}$ (two equilibrium positions).
To achieve two symmetric equilibrium positions ($\theta_1=-\theta_2$) we adjust two screws to trim the tensions of the two lateral springs.
To study the forced oscillations we attached to the brass disc one end of an helicoidal spring (wound around the axis). The other spring end is driven through a drag-link by a d.c. motor with adjustable speed. By changing the arm of the drag-link or the motor speed we may adjust the amplitude or the frequency of the driving torque $K\theta_f$, where K (Nm/rad) is the spring torsion constant and θ_f is the angular displacement of the helicoidal spring end, measured by a rotational potentiometer (see figure 5).
The motion of the spring end attached to the drag-link is approximately sinusoidal, so that the forced pendulum is described by the equation:

$$I\frac{d^2\theta}{dt^2} = \pm MgR\sin\theta - K_{eff}\theta - 2\gamma\frac{d\theta}{dt} + K\theta_f\cos(\omega t) \qquad (9),$$

where the sign + refers to the case of inverted pendulum and the sign – to the case of normal pendulum.
The effective torsion constant K_{eff} that in equation (9) gives the restoring torque $T=K_{eff}\theta$ is produced both by the lateral springs and by the helicoidal spring. The lateral springs apply forces at the distance r from axis, so that: $K_{eff}=(k_1+k_2)r^2+K$.
Approximating $\sin\theta$ with the first two term in McLaurin series expansion ($\theta - \theta^3/6$), (that is a good approximation up to $\theta=1$ rad) equation (9) turns into Duffing equation.
In fact letting:

$$\begin{aligned}\alpha &= \left[K_{eff} \pm MgR\right]/I\ ,\\ \beta &= \mp MgR/6I\ , \qquad (10)\\ \varepsilon &= 2\gamma/I\ ,\\ F_\theta &= K\theta_f/I\ ,\end{aligned}$$

(where upper sign refers to normal pendulum and lower sign refers to inverted pendulum) we obtain:

$$\frac{d^2\theta}{dt^2} + \varepsilon\frac{d\theta}{dt} + \alpha\theta + \beta\theta^3 = F_\theta\cos(\omega t) \qquad (11).$$

that equals equation (4) if the variable x is replaced by θ and the term F/M is replaced by F_θ.
Within the limits of our approximation we expect that, in *stationary* forced oscillations (the stable oscillations surviving after the transient is died out), for each value of the amplitude two different values $\omega_{1,2}$ of the angular frequency are possible. These values are the solutions of the equation (5):

$$\omega_{1,2}^2 = (\alpha+3/4\beta A^2-\varepsilon^2/2) \pm \sqrt{\varepsilon^4/4 - \varepsilon^2(\alpha+3/4\beta A^2) + F_\theta^2/A^2} \qquad (12)$$

We also expect that *free* oscillations satisfy the relation:

$$\omega^2 = \alpha + 3/4\ \beta\ A^2 \qquad (12').$$

Our approximated model predicts for the phase angle ϕ (between stationary oscillation and driving torque) the relation:

$$\tan\Phi = \frac{\varepsilon\omega}{\alpha - \omega^2 + (3/4)\beta A^2} \qquad (13\ ).$$

May be useful to note the dimensions of the parameters in relations (11), (12), (13): $[\alpha]=[\beta]=[F_\theta]=s^{-2}$, $[\varepsilon]=s^{-1}$. We also note that in relation (13) the phase ϕ depends both on ω and on A, and that the angular frequency ω, is a *twofold* function of the amplitude A through relation (12).

2. Evaluation of the apparatus parameters

To evaluate the elastic constant k_1, k_2, we measured the change in length of the lateral springs under known loads.
To evaluate the inertial momentum I we weighted and measured the geometry of all components of the pendulum. The accuracy of this evaluation was checked by comparing the calculated value of I with the experimental value obtained from the measurement of the period of free oscillations of the pendulum without eccentric mass and without helicoidal spring (compensating the missing mass m_{slot} due to the slot in the disc with a small added mass that cancels the gravitational restoring torque).
Details and results of these measurements are reported hereafter

2.1 Elastic constants k_1, k_2, K and momentum of inertia I

The calculated momentum of inertia is I_{calc} =(1.87 ± 0.06) 10^{-3} kg m^2, in good agreement with the value obtained from the measured period T = (1.49 ± 0.01) s and the measured values of the elastic constants k_1 = (316 ± 9) N/m and k_2 = (313 ± 5) N/m. From relation $(2\pi/T)^2 = (k_1 + k_2)r^2 / I$ we get in fact I = (1.86±0.09) 10^{-3} kg m^2.
With the eccentric mass (M = 107.1 g) placed at R_{min}= (43 ± 1) mm we get: $I_{total} = I + M R_{min}^2$ = (1.975 ± 0.06) 10^{-3} kg m^2
In the same condition the gravitational torque (accounting for $m_{slot}\approx$ 6 g, and assuming the missing mass to be concentrated on the mean radius r_m=54 mm) is $MgR' = MgR_{min} - m_{slot}\ g\ r_m$ = (0.042 ± 0.001) Nm.
The torsion constant K of the helicoidal spring is indirectly evaluated comparing the free oscillation periods of the pendulum without any eccentric mass, the one due to the lateral springs T_1 = (1.49 ± 0.01) s and the one due to the axial helicoidal spring T_2 = 2.12 ± 0.03 s.
The ratio between the two torsion constants must equal the square of the inverse ratio of the two periods:

$$K / \left[(k_1 + k_2) r^2 \right] = \left(T_1 / T_2 \right)^2 = 0.493 \pm 0.007.$$

where r is the axis radius (r = 7.25 ± 0.10 mm). This gives K = (1.63 ± 0.06) 10^{-2} Nm/rad, and $K_{eff} = (k_1 + k_2)r^2 + K$ = (4.94 ± 0.15) 10^{-2} Nm/rad.

2.2 The friction coefficient ε

A record of the amplitude of the free oscillations (with no eccentric mass) as a function of time is reported in Figure 7.
The experimental behaviour cannot be well fitted by the exponential decay predicted by Duffing equation: at small amplitudes the oscillations damping is approximately linear (as in the case of velocity independent friction).
However, by fitting the experimental data with the Duffing model we obtain at least an approximate evaluation of the decay constant $\gamma/I \approx 0.18$ s^{-1} , i.e. $\varepsilon = 2\gamma/I \approx 0.36$ s^{-1}.

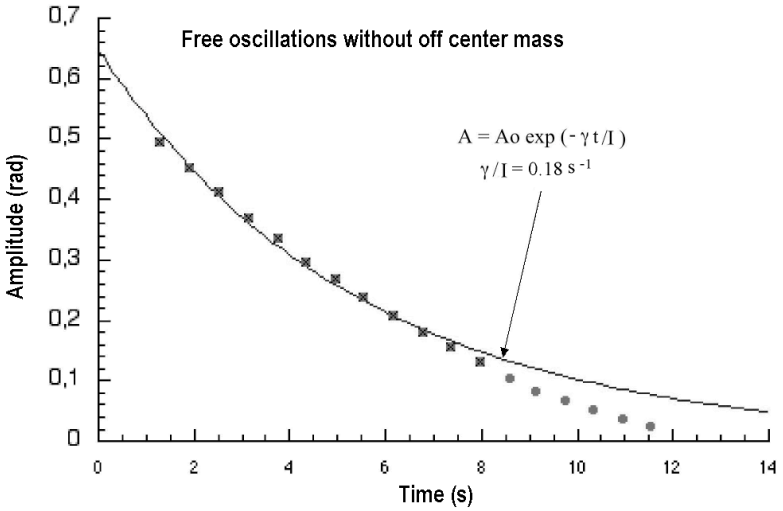

Figure 7: Free oscillation amplitude as function of time. Dots: experimental results. Line: exponential best fit to points at large amplitude.

2.3 Nominal values of the parameters α and β in Duffing equation

Using the calculated values of I, K, k_1, k_2 in relations (10) we get the nominal values for the parameters α and β of Duffing equation. For $R = R_{min}$, in the two cases of normal and inverted pendulum we obtain:

$\alpha_{norm} = [K + (k_1+k_2)\, r^2 + MgR'] / I = (46.3 \pm 1.6)\ s^{-2}$

$\alpha_{inv} = [K + (k_1+k_2)\, r^2 - MgR'] / I = (3.7 \pm 1.0)\ s^{-2}$

$\beta_{norm} = - MgR'/(6\, I) = - (3.5 \pm 0.2)\ s^{-2}$

$\beta_{inv} = + MgR'/(6\, I) = + (3.5 \pm 0.2)\ s^{-2}$

3. Experimental results and data analysis

We first studied the free damped oscillations whose frequency does strongly depend on the amplitude. Then we investigated the forced oscillations, by keeping the driving force at small value in order to be able to observe, after a transient, a stationary motion with a period identical to that of the driving force (the so-called *harmonic* oscillations). In this configuration we observed the phenomenon of amplitude jumps, associated to hysteresis.

By increasing the driving force we than produced *subharmonic* oscillations (whose period is longer than that of the driving force). Finally, further increasing the amplitude we observed the *transition to chaotic motion*.

Predictions based on nominal values of the parameters and on approximate equations (12) and (12') are compared to experimental results for free and forced oscillations, both in the case of normal and of inverted pendulum.

One may obviously expect that approximate prediction will match experimental results only for small amplitudes.

To match experimental data at larger amplitudes we must proceed to numerical integration of the exact motion equation (4), e.g. using commercial software for modelling as Stella [12].

The results of numerical simulations are reported in section 4.

3.1 The normal pendulum

The experimental dependence on amplitude of the *free oscillations* frequency is reported in Figure 8.

The more the oscillation is damped the more its (pseudo)period decreases, following approximately the behaviour predicted by relation (12') with the nominal values of α and β.

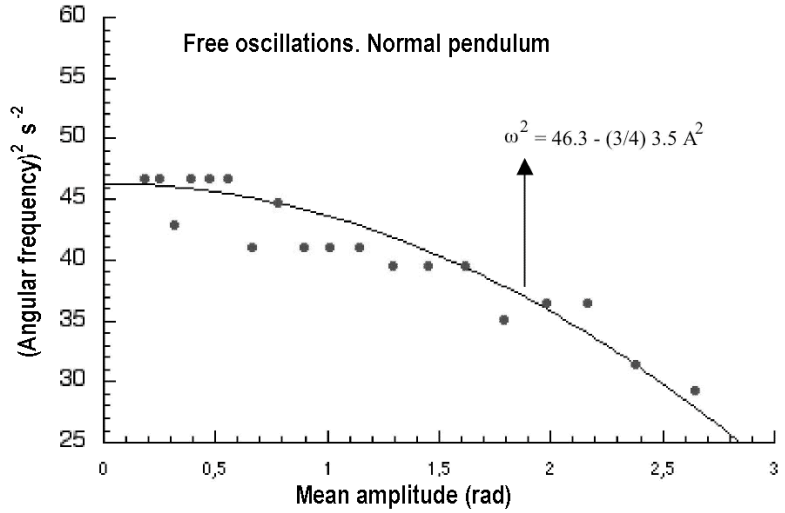

Figure 8: the square of the angular frequency as a function of amplitude of the free oscillations of normal pendulum (β<0).

The *forced oscillations* were studied using for the helicoidal spring a driving amplitude θ_f=0.6 rad, by gradually changing the frequency of the driving torque (either increasing or decreasing it), and always *waiting for stabilization of the oscillation amplitude.*
As shown in figure 9 and 10 (where in the vertical axis we plot the frequency instead of the square of angular frequency), this procedure leads to hysteresis in the resonance curve, and to the phenomenon of amplitude jumps.

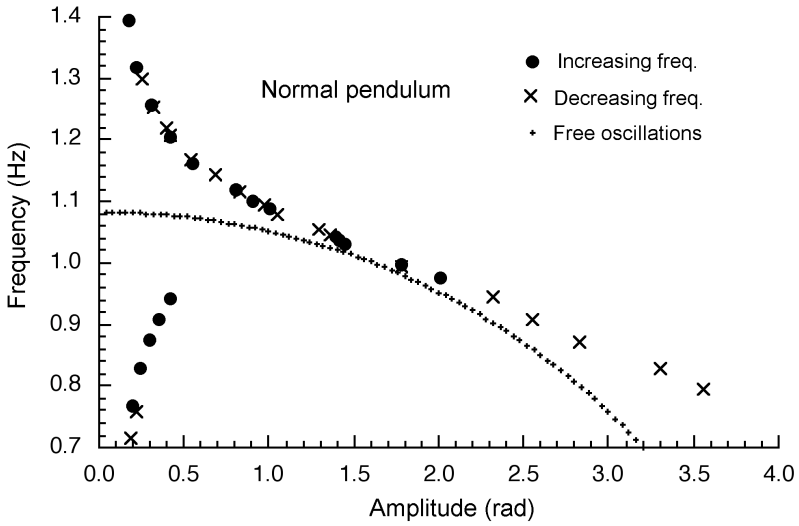

Figure 9: Experimental relation between frequency and amplitude of forced oscillations in normal pendulum (β<0); increasing frequency (×) and decreasing frequency (✺). Dotted line shows the predicted behaviour of free oscillations.

By using equation (12), the evaluated α, β and ε parameters, the measured θ_f (that gives $F_\theta = K\theta_f / I = (5.0 \pm 0.3)\ s^{-2}$), we may graph the experimental resonance curve (figure 10). We see that the approximated model, using the nominal values of the

parameters α , β, ε and F_θ, is in fair agreement with experimental results up to about 2 rad,

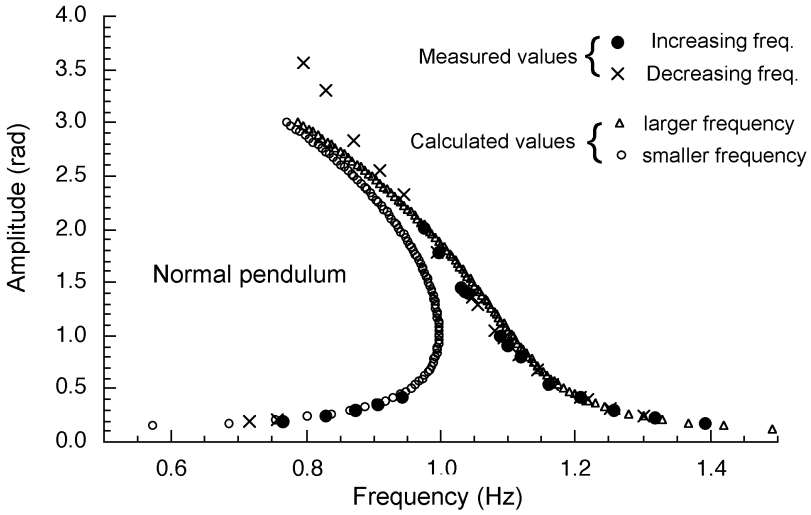

Figure 10: comparison of the approximated theory with experimental data for normal pendulum ($\beta<0$)

We also measured the phase angle Φ between the driving torque and the stationary oscillation as a function of frequency (figure 11).
Because in equation (13) Φ depends both on amplitude and frequency, to calculate the curve shown in figure 11 we first calculate for each amplitude the corresponding two values of frequency through equation (12) and then we insert them into (13) to obtain $\Phi_{1,2}$.

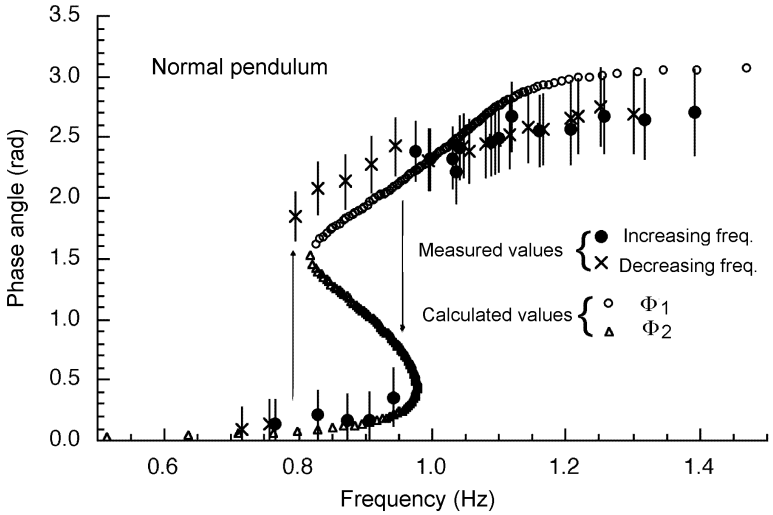

Figure 11: Phase angle measured increasing (●) and decreasing (×) frequency, compared with the values $\Phi_{1,2}$ calculated from approximated theory

We observe that the phase angle is nearly zero at the lower frequencies (oscillations *in phase* with the driving torque) and nearly π at the higher frequencies (oscillations *in opposition* with the driving torque).

3.2 Inverted pendulum

In the case of inverted pendulum, the free oscillations damp much faster than in the case of normal pendulum because the restoring torque is now the *difference* (and not

the *sum*) of elastic and gravitational torques, so that the ratio between restoring torque and friction torque is smaller.
Therefore, in order to record at least 5 complete oscillations, one must start with initial amplitude close to 4 rad: this makes impossible to use equation (12') as a good approximation of experimental data. Figure 12 shows in fact that the agreement is fair only at small amplitude.

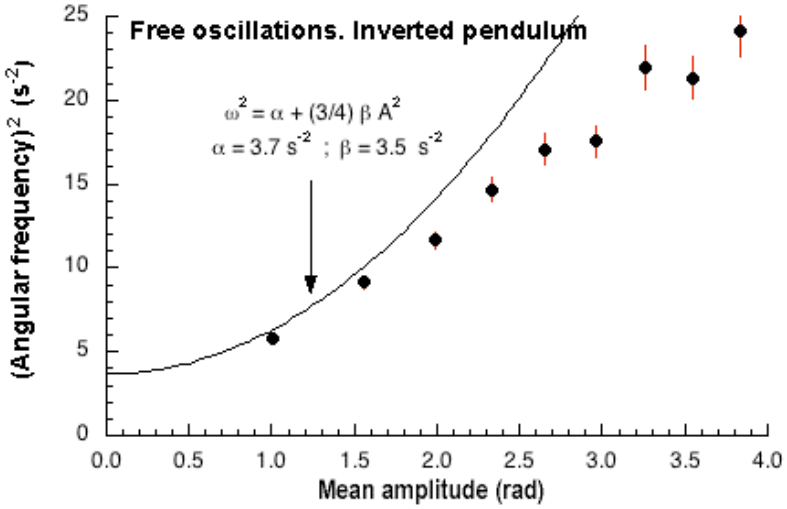

Figure 12: the square of the angular frequency as a function of amplitude of the free oscillations of inverted pendulum (β>0).

By driving the inverted pendulum with an amplitude θ_f=0.6 rad we obtain the results shown in Figure 13. Here the data are plotted as a resonance curve together with the predicted values calculated from the approximate model (12).

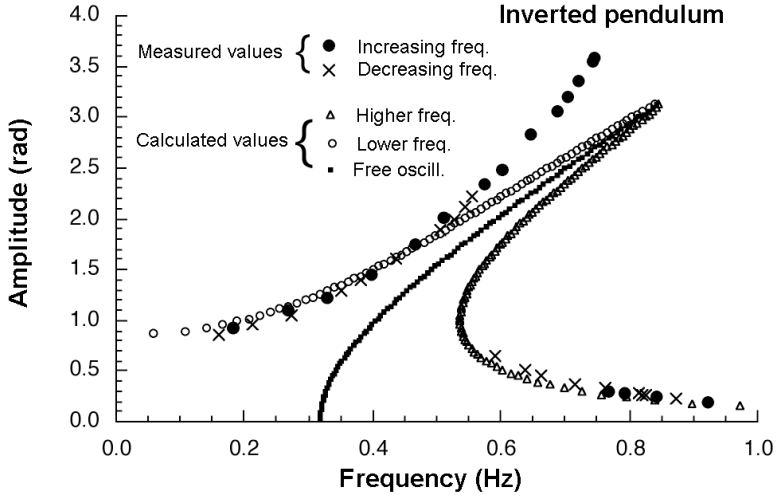

Figure 13: Resonance curve of the inverted pendulum (β>0). The calculated values are obtained from the approximate theory

4. Numerical simulation

We used a simulation software widely used in education (Stella [12]), that *numerically* integrates equation (4) using Euler method (or Runge-Kutta method) giving the solution both in graphic and in table format.
We used the time interval between steps Δt=5 ms, a choice adequate to faithfully reproduce the damped harmonic oscillations (that can be solved also analytically).
The equation to be numerically solved is:

$$\frac{d^2\theta}{dt^2} \pm MgR/I \sin\theta + K_{eff}/I\ \theta + 2\gamma/I \frac{d\theta}{dt} = K\theta_f/I \cos(\omega t) \qquad (14)$$

where the + sign is for the case of normal pendulum and the – sign for the case of inverted pendulum. In the simulation we used for the parameters the following values: $MgR/I = 20.6\ s^{-2}$, $K_{eff}/I = 25.0\ s^{-2}$, $2\gamma/I = 0.35\ s^{-1}$, $F_\theta = K\theta_f/I = 4.8\ s^{-2}$.

To obtain the curve with increasing frequency, the initial conditions were $\theta_{(t=0)} = 1$ and $d\theta/dt_{(t=0)} = 0$, and, for each driving frequency, the amplitude obtained after at least 50 cycles was recorded. The curve with decreasing frequency was similarly obtained by changing the initial conditions with a trial and error procedure (figures 14 and 15).

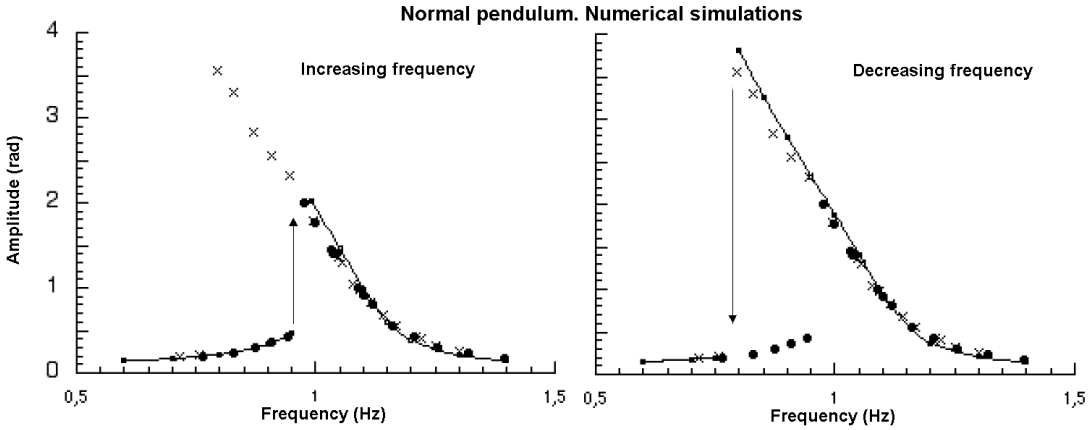

Figure 14: Normal pendulum: numerical simulations for increasing and decreasing frequencies (line) compared with experimental results

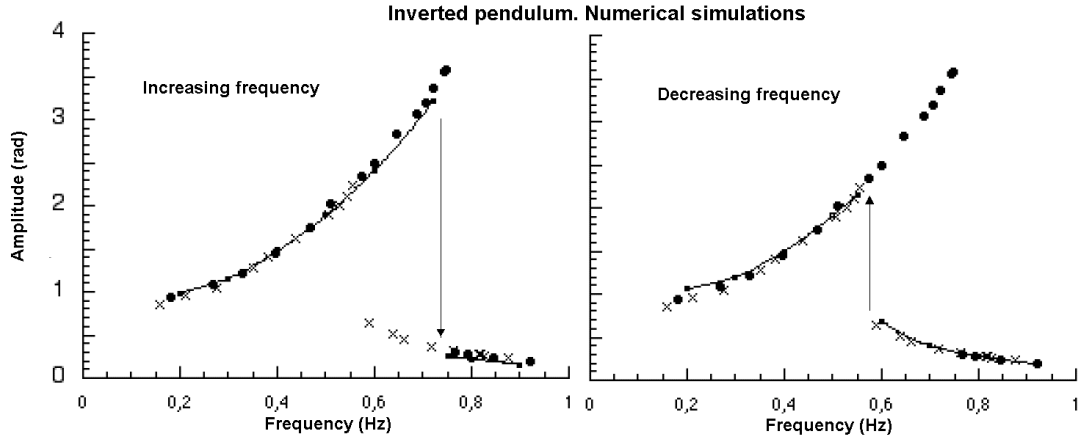

Figure 15: Inverted pendulum: numerical simulations for increasing and decreasing frequencies (line) compared with experimental results

The advantage of *numerical integratio*n is apparent: now also the values calculated for *large amplitudes* are in good agreement with the measured values.

5. Transition to chaos

Several simulation studies in the literature (e.g. [8], [9], [10], [11]) point out a general feature of non linear systems described by Duffing equation: by slightly varying the amplitude *f* of the driving force (at a frequency close to the self frequency $\omega_o = \sqrt{|\alpha|}$) starting from *very small amplitude* the system stationary state is a periodic motion synchronous with the driving force (harmonic oscillation); by increasing the driving force beyond a first threshold value f_1, the stationary oscillation has a period that

doubles the driving period. Further increase of the driving force brings to a cascade of *period doubling* corresponding to threshold values $f_2, f_3, \ldots f_n$ converging to a limit value f_c in a series described by Feigenbaum equation

$$\lim_{n\to\infty} \frac{f_{n+1} - f_n}{f_{n+2} - f_{n+1}} = \delta = 4.6692\ldots..$$

For driving forces greater than f_c the system cannot reach stationary periodic motion; it exhibits non periodic (chaotic) oscillations that, for extremely small changes in the initial conditions, evolve in completely different (unpredictable) orbits in the phase.
This behaviour may be depicted in a graph (*bifurcation plot*), as that shown in Figure 16 taken from [8] and generated by a restoring force with both linear and cubic terms ($\alpha < 0$ and $\beta > 0$) , i.e. with two stable equilibrium positions (the same as inverted pendulum with $MgR > K_{eff}$).

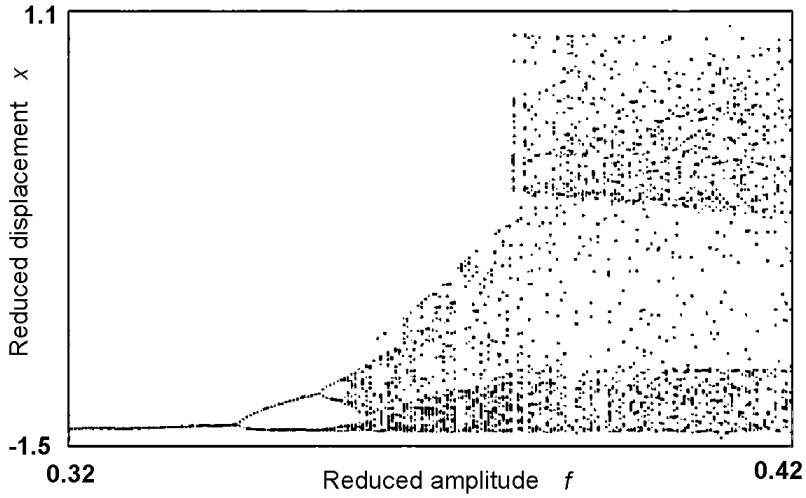

Figure 16: A bifurcation plot taken from [8]

In figure 16 the abscissa represents the driving force amplitude f (in reduced units) and the ordinate represents the displacement x (in reduced units) from equilibrium position recorded at a given time for each period.
Up to $f = 0.34$ the motion shows a single period (small oscillation around an equilibrium position) and it is therefore represented in the plot by a single dot.
For $0.34 < f < 0.35$ the first *period doubling* appears and the plot *bifurcates* , i.e. for each f value we have two values for x.
Further increase of f leads to a series of bifurcations (*subharmonic oscillations of order n*) and the stationary oscillation period becomes T_f^n, if T_f is the driving force period. Beyond a critical value of the driving amplitude $f_c = 0.361$, chaotic motion appears.
Using reduced units simplifies the Duffing equation into the form:

$$d^2x/d\tau^2 + \varepsilon\, dx/d\tau + x + x^3 = f\cos(\omega\tau)$$

where all variables and parameters are pure numbers. To achieve this form we may proceed as follows. Starting from the motion equation of a mass M moving along y axis with a (linear + cubic) restoring force:

$$d^2y/dt^2 + \varepsilon\, dy/dt + \omega_o^2\, y + \beta\, y^3 = f\cos(\omega t).$$

where $f = F/M$, F is the driving amplitude, and ω is the angular frequency we obtain the following dimensions: $[\varepsilon] = s^{-1}$, $[\beta] = s^{-2}m^{-2}$, $[\omega] = [\omega_o] = s^{-1}$, $[f] = N\,kg^{-1} = m\,s^{-2}$
Letting $\tau = a\,t$, and $x = b\,y$, the equation becomes:

$$(a^2/b)\, d^2x/d\tau^2 + \varepsilon\,(a/b)\, dx/d\tau + (\omega_o^2/b)\, x + (\beta/b^3)\, x^3 = f \cos(\omega\tau/a).$$

Multiplying by b/a^2 we get

$$d^2x/d\tau^2 + \varepsilon/a\, dx/d\tau + (\omega_o^2/a^2)\, x + \beta/(a^2b^2)\, x^3 = f\, b/a^2 \cos(\omega\tau/a).$$

By choosing $a = \omega_o$ and $b^2 = \beta/a^2 = \beta/\omega_o^2$

And using the reduced variables x, τ , ε', ω' and f':

$$\varepsilon' = \varepsilon / \omega_o, \qquad f' = f\,\beta^{1/2} / \omega_o^3$$
$$\omega' = \omega / \omega_o \qquad (14)$$
$$\tau = \omega_o\, t \qquad x = (\beta^{1/2} / \omega_o)\, y.$$

the equation becomes

$$d^2x/d\tau^2 + \varepsilon'\, dx/d\tau + x + x^3 = f' \cos(\omega'\, \tau),$$

Using this form of Duffing equation makes much easier the numerical simulation: we use only three parameters: reduced friction coefficient ε', reduced amplitude f' and reduced driving frequency ω'. The data reported in figures 14 and 15 were obtained letting $\omega' = 1$, $\varepsilon' = 0.5$ and varying only f'.

Despite the *non-periodic* behaviour of the pendulum, in the chaotic regime some regularity appears if we represent it in a *Poincaré map*.

The Poincaré map is a special bidimensional phase plot (θ, ω) (i.e. angular position versus angular velocity) where each dot describes the state of the system recorded once for each period, at the same time (for example when the driving force assumes the maximum positive value).

For a simple harmonic motion the Poincaré map reduces to a single dot. For subharmonic oscillations of order n we get n dots, while for chaotic motion the number of dots diverges.

These dots however are not randomly placed in the (θ,ω) plane: they build a *fractal pattern* that takes the name of *strange attractor*, or *chaotic attractor* . An example is reported in figure 17, taken from [7], that refers to the normal pendulum with $\omega' = 2/3$, $\varepsilon' = 0.25$ and $f' = 1.5$.

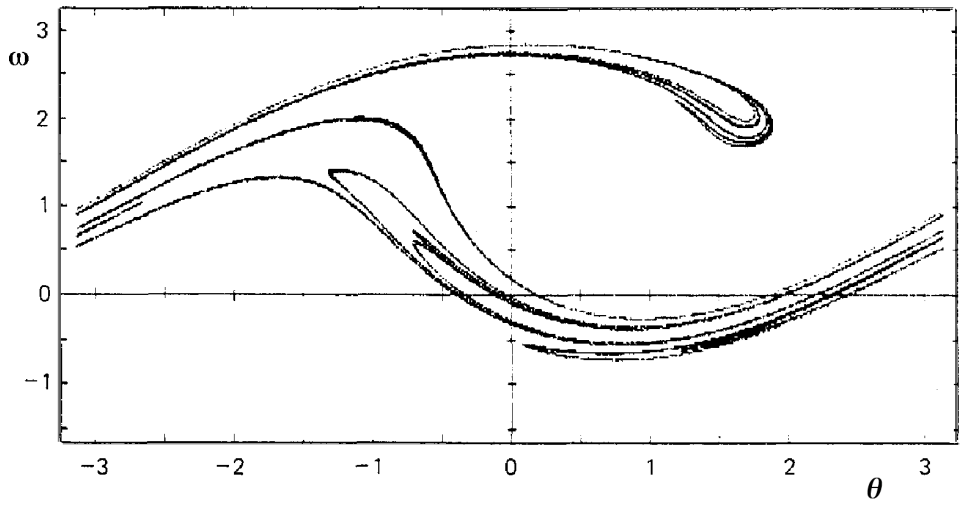

Figure 17 : Example of Poincarè map taken from [8]

In our torsion pendulum it is not easy to trim the driving amplitude (we should radially displace the pivot of the drag-link on the disc attached to the motor), while we may easily adjust the driving frequency, by simply changing the voltage supplied to the d.c. motor

Therefore we worked at constant driving torque and we changed the driving frequency looking for frequencies at which period doubling appears.

The eccentric mass was fixed at a distance R=59 mm from axis, to obtain $\alpha<0$, i.e. MgR (= 0.0588 Nm) > K_{eff} = 0.0494 Nm. The two equilibrium position are in this case at $\theta_{1,2} = \pm\sqrt{6(1 - K_{eff} / MgR)} = \pm$ 0.98 rad.

Some examples of the different behaviours (all obtained using a small driving amplitude θ_f = 0.57 rad) are given in the following.

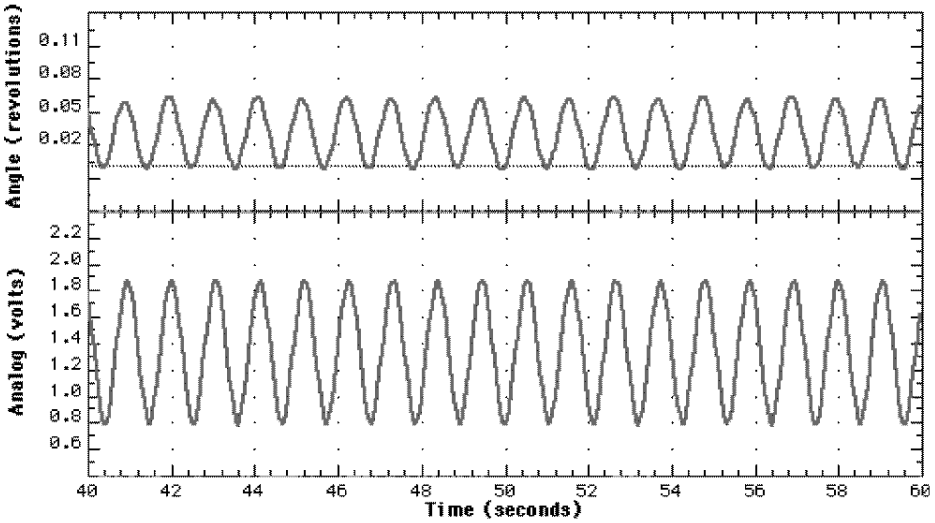

Figure 18: Oscillations around one of the two stable equilibrium positions. Upper plot: the pendulum angular displacement, lower plot: output voltage of the sensor measuring the driving torque.

At the driving frequency ν = 0.94 Hz, oscillation is synchronous with the forcing torque (figure18). A Fourier analysis confirms the presence of a single frequency, and the phase plot (θ , ω) is a single loop (Figure 19), slightly deformed due to uncertainties in the computation of angular velocity (data taken at low acquisition rate)

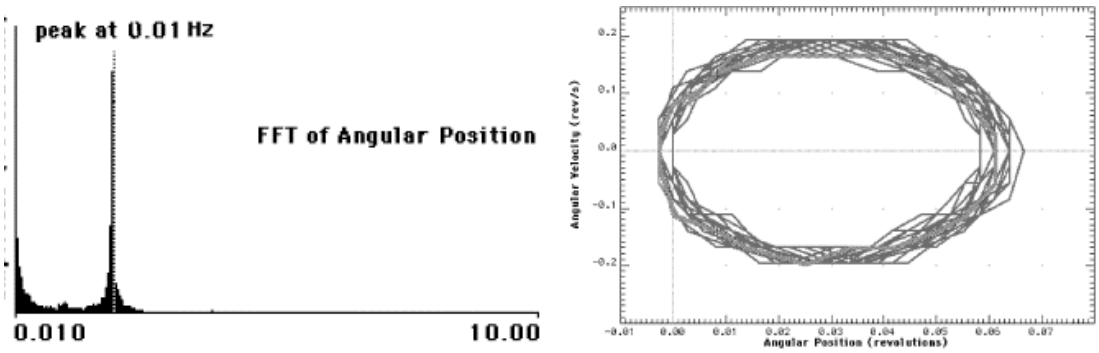

Figure 19: Oscillations around one of the two stable equilibrium positions. At left the Fourier spectrum, at right the phase space plot.

At ν = 0.84 Hz, we still observe a stable periodic oscillation, but now the period is doubled, and the Fourier analysis shows two peaks: one at the driving frequency and one at half that frequency (Figure 20).

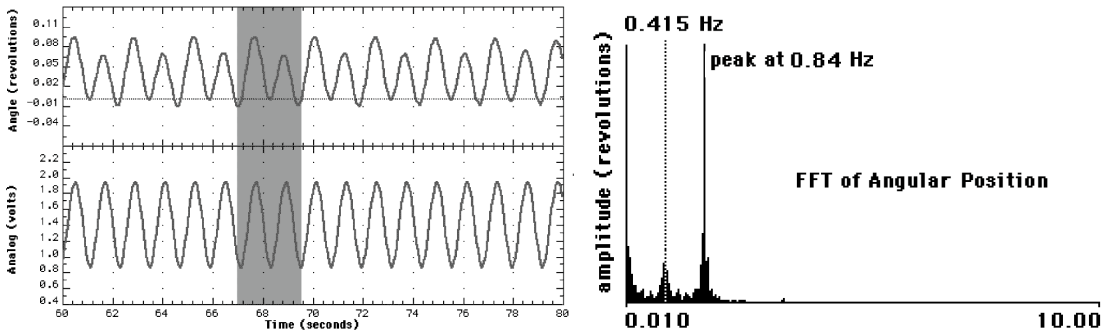

Figure 20: Period doubling. At left the time evolution, at right the Fourier spectrum: two peaks at 0.84 Hz and 0.415 Hz

The phase space plot shows two intersecting loops and the numerical simulation with Stella does well reproduce the experimental pattern (Figure 21),

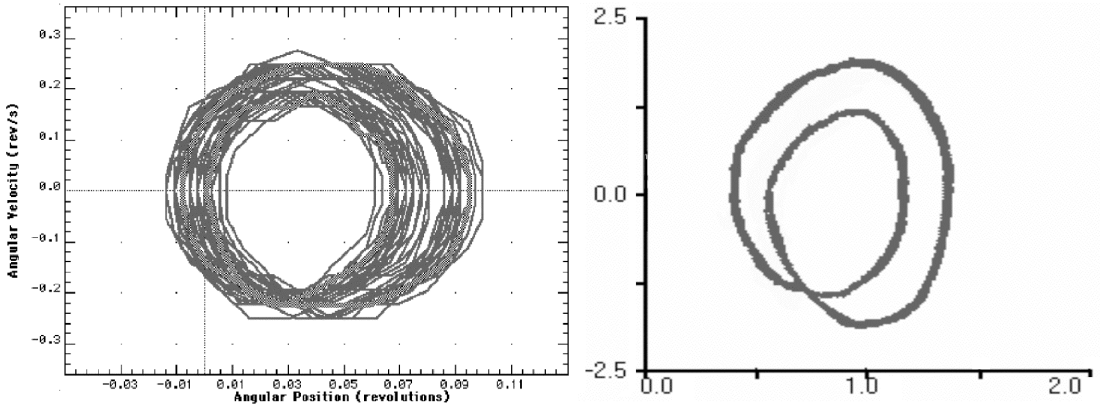

Figure 21: Period doubling in the phase space plot. At left the experimental data , at right the numerical simulation.

At $\nu = 0.76$ Hz, we observe oscillations with a period that is *four times* the driving period (Figure 22)

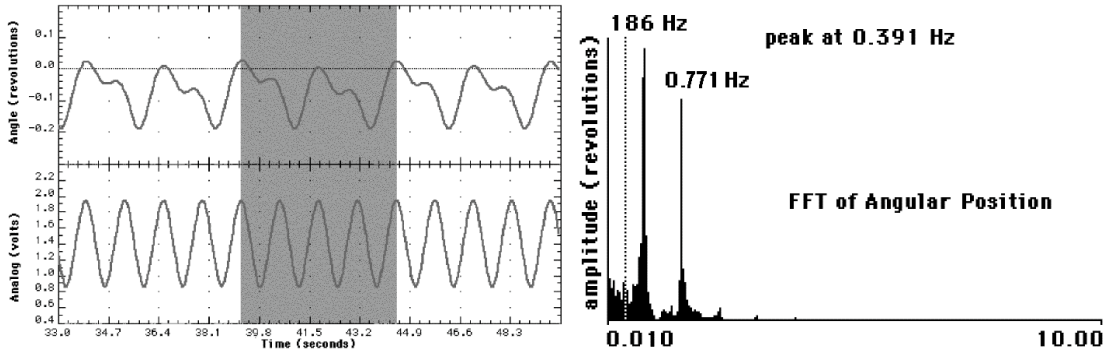

Figure 22: Second period doubling. At left the time evolution, at right the Fourier spectrum: three peaks at 0.186, 0.391 and 0.771 Hz

The Fourier spectrum shows indeed peaks at 1/2 and 1/4 of the driving frequency, and the Stella simulation gives a plot in phase space similar to the experimental one (Figure 23)

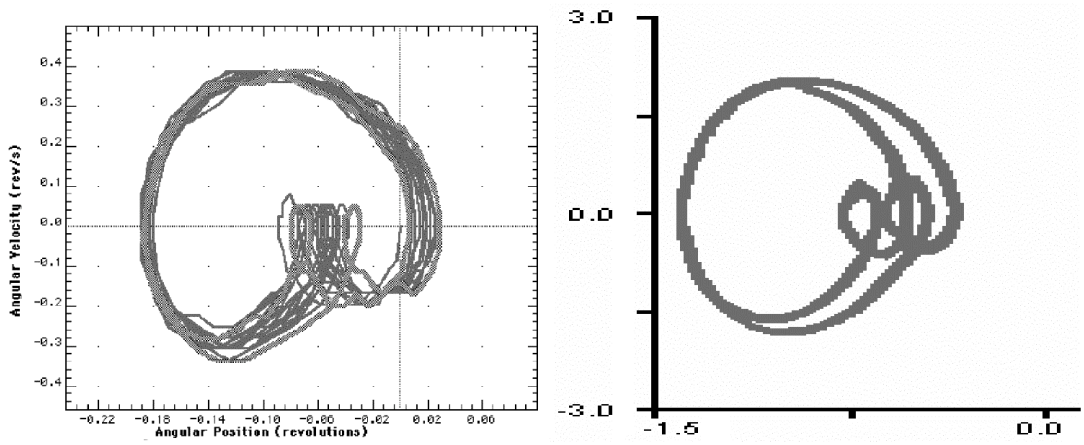

Figure 23: Second period doubling in the phase space plot. At left the experimental data, at right the numerical simulation.

At $\nu = 0.70$ Hz we observe the transition to chaotic regime (figures 24 and 25) where the pendulum oscillates for a while around one equilibrium position, and then jumps to oscillation around the other equilibrium position, in a random way.

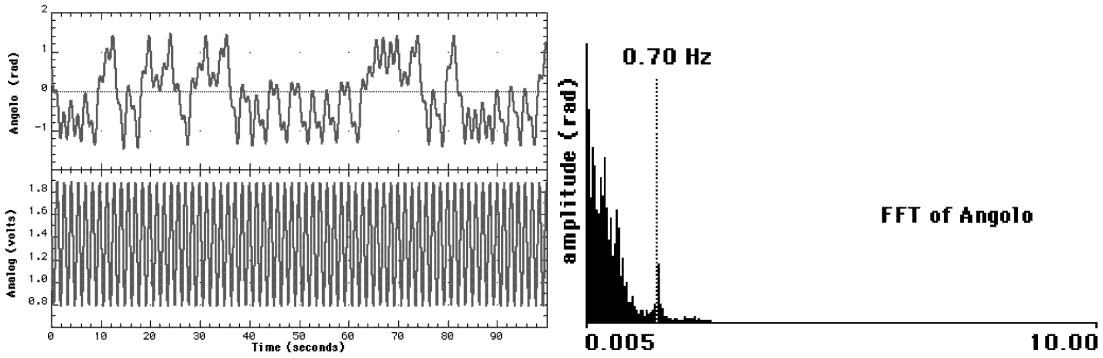

Figure 24: Chaotic motion. At left the time evolution, at right the continuous Fourier spectrum with a peak at the driving frequency.

The Fourier transform gives a substantially continuous spectrum, from which emerges a peak at the driving frequency, and the plot in space phase obtained by numerical simulation reproduces well the experimental one (figure 25) .

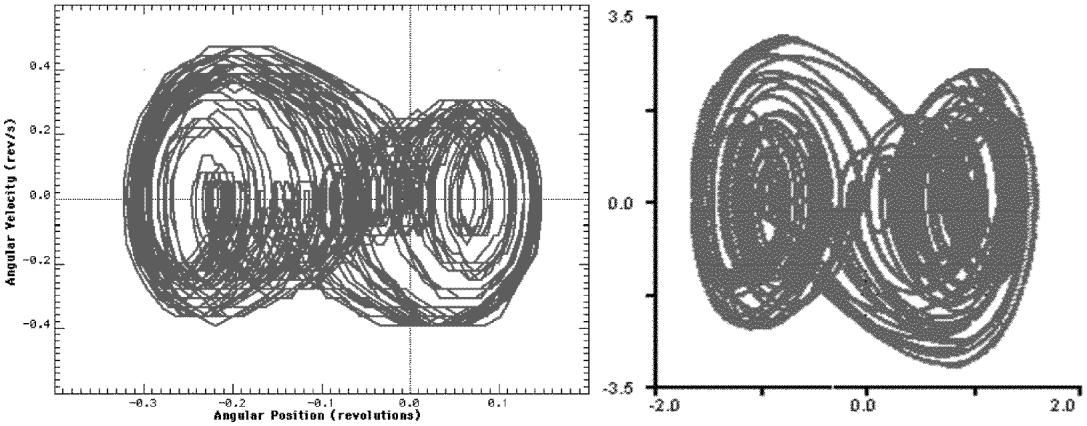

Figure 25: Chaotic motion in the phase space plot At left the experimental data, at right the numerical simulation.

The Poincaré map, taken by recording θ and ω values corresponding to the positive maximum of the driving torque is shown in Figure 26: at left the experimental one and at right the one numerically simulated.:

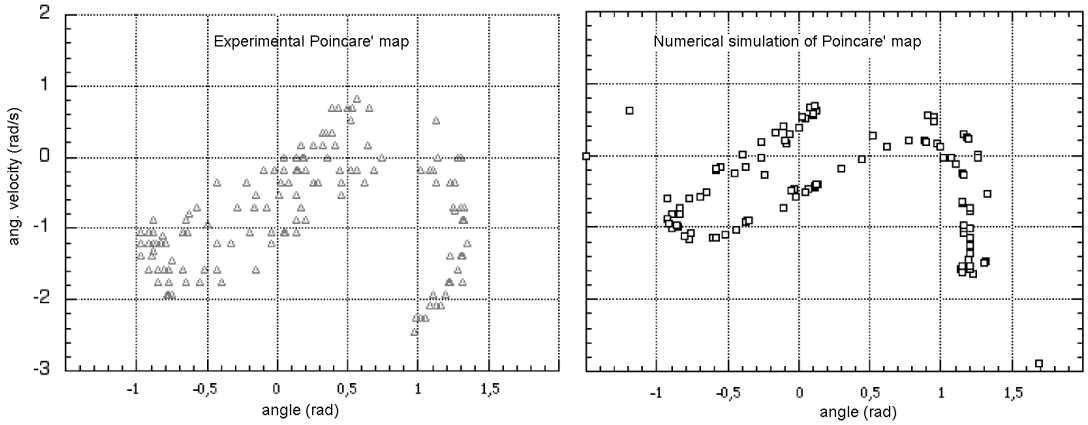

Figure 26: Poincaré map . At left the experimental data, at right the numerical simulation

We also observed a period triplication at ν = 0.51 Hz (figures 27 and 28). This feature may be found within one of the periodic windows in the chaotic region [7],

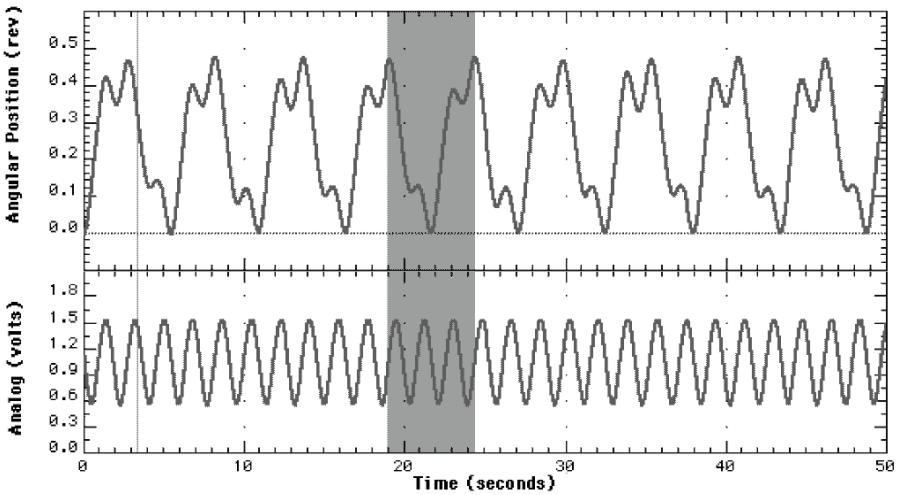

Figure 27: Stable oscillations at a period three times the driving period.

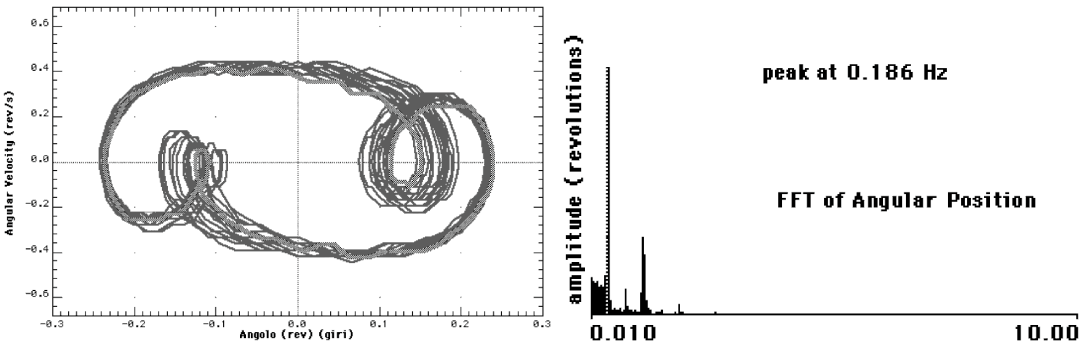

Figure 28: Third subharmonic. At left the phase space plot, at right the Fourier spectrum: the highest peak is at frequency 1/3 of the driving frequency

6. "Historical" remarks, acknowledgements and a bibliographic list

The idea of this didactical apparatus was born during a discussion of one of the authors (G.T.) with prof. Arturo Loria after the 30th International Physics Olympiad held in Padua in 1999, about the problem on inverted torsion pendulum assigned to the students as part of the experimental competition. The very simple device given to the students was cleverly designed by Edoardo Miletti [13] in order to allow either horizontal or vertical rotation axis, and the torque of the eccentric mass could be adjusted by screwing or unscrewing the threaded pendulum rod, thus allowing to vary the system behaviour and showing bifurcation.
Prof. Loria (who was aware of the various computer-assisted experiments previously designed by the authors for didactic laboratory) suggested us to setup an apparatus that could make possible both *real time data acquisition* of the system evolution and *controlled forced oscillation*s, in order to exploit the full range of educational use of this interesting device.
Our first step was to prepare a prototype on which Samo Lasic's thesis was based, demonstrating essentially all the features described in the present paper. The numerical simulations, as well as a more complete analysis of the system, were performed within the thesis later assigned to Paola Bedendo.
The result is an experiment that, using simple and cheap tools, allows to fully investigate both linear and non-linear oscillators with a complete control of all the interesting parameters.
Both approximate-analytical and exact-numerical solutions of the Duffing oscillator may be tested in comparison with experimental measurement, leading to a deeper understanding of complex phenomena.
In order to make easier to the reader a comparison of our apparatus with similar systems described in the literature, we add hereafter a list of references on this topic, in chronological order.

T. W. Arnold, W. Case, *Nonlinear effects in a simple mechanical system*, Am. J. Phys. **50** (1982)

K. Luchner, *Chaotic motion: Mechanical systems in experiment and simulation,* Bild der Wissenschaft **4** (1983)

H. J. Janssen, R. Serneels, L. Beerden, E. L. M. Flerackers, *Experimental demonstration of the resonance effect of an anharmonic oscillator*, Am. J. Phys. **51** (1983)

K. Briggs, *Simple experiments in chaotic dynamics*, Am. J. Phys. **55** (1987)

B. Duchesne, C. W. Fischer, C. G. Gray, K. R. Jeffrey, *Chaos in the motion of an inverted pendulum: An undergraduate laboratory experiment*, Am. J. Phys. **59** (1991)

N. Alessi, C. W. Fischer, C. G. Gray, *Measurement of amplitude jumps and hysteresis in a driven inverted pendulum*, Am. J. Phys. **60** (1992)

R. Cuerno, A. F. Ranjada, J. J. Ruiz-Lorenzo, *Deterministic chaos in the elastic pendulum: A simple laboratory for nonlinear dynamics*, Am. J. Phys. **60** (1992)

K. Weltner, A. S. C. Esperidiao, R. F. S. Andrade, G. P. Guedes, *Demonstrating different forms of the bent tuning curve with a mechanical oscillator*, Am. J. Phys. **62** (1994)

R. D. Peters, *Chaotic pendulum based on torsion and gravity in opposition*, Am. J. Phys., **63** (1995)

A. Siahmakoun, V. A. French, J. Patterson, *Nonlinear dynamics of a sinusoidally driven pendulum in a repulsive magnetic field*, Am. J. Phys. **65** (1997)

A. Prosperetti, *Subharmonics and ultraharmonics in the forced oscillations of weakly nonlinear systems*, Am. J. Phys. **44** (1997)
B. K. Jones, G. Trefan, *The Duffing oscillator: A precise electronic analog chaos demonstrator for the undergraduate laboratory*, Am. J. Phys., **69** (2001)

References

[1] G. Duffing *Erzwungene Schwingungen bei veränderlicher Eigenfrequenz*, F.Wieweg u. Sohn, Braunschweig (1918)
[2] J.J. Stoker: *Nonlinear vibrations in Mechanical and Electrical Systems*, Interscience Publishers (1950)
[3] S. Lasic: *Didactical treatment of torsion pendulum with the transition to chaos* , Thesis, University of Ljubljana, Faculty for Mathematics and Physics, 2001
[4] S. Lasic , G. Planinsic, G.Torzo : *Torsion pendulum: a mechanical nonlinear oscillator*, Proceedings GIREP 2001, Udine (2001)
[5] P. Bedendo: *Oscillatori lineari e non-lineari e fenomeni caotici,* Tesi di laurea , Padova, 2002
[6] Home-made sensor equivalent to Rotary Sensors produced by MAD (http://www.edumad.com), PASCO (http://www.pasco.com), Vernier Software (http://www.vernier.com) and LABTREK (http://www.labtrek.net)
[7] We used the ULI interface from Vernier (http://www.vernier.com), with software RotaryMotion for Macintosh. Identical results may be obtained with similar interfaces (e.g. Vernier-LabPro, Pasco-CI500)
[8] G. L. Baker and J. P. Gollub: *Chaotic Dynamics, an introduction*, Cambridge University Press, 1990
[9] M. Lakshmanan e K. Murali: *Chaos in Nonlinear Oscillators* World Scientific 1996, Cap 4
[10] M. Lakshmanan e K. Murali: Physics News **24**, 3 (1993)
[11] C. L. Olson, M. G. Olsson, *Dynamical symmetry breaking and chaos in Duffing's equation*, Am. J. Phys. **59** (1991)
[12] Stella Research, vers. 5.1, software distributed by *High Performance Systems Inc.*, http://www.hps-inc.com
[13] E. Milotti: *Non linear behaviour in a torsion pendulum*, Eur. J. Phys. **22** (2001)